Surface Load Induced Earthquakes

Amanda Syamsul* and Bradley Paul Lipovsky

Department of Earth and Space Sciences, University of Washington
Seattle, Washington, USA

*To whom correspondence should be addressed; E-mail: amand4@uw.edu.

Loads on the surface of the Earth modify earthquake occurrence. Previous studies of this phenomenon have been limited in geographical and temporal extent. Here, we systematically search global datasets for a relationship between surface mass loading and earthquake occurrence. Using a non-parametric, Bayesian analysis we confirm that surface loading during periods with an earthquake differs significantly from the background. This result is insensitive to earthquake catalog declustering. We find the highest relative probability of earthquake occurrence at locations undergoing extreme surface mass loading and unloading.

Introduction

Although the dominant forcing for earthquakes is plate tectonics, surface loads acting on the surface of the Earth such as changes in lake, reservoir, or ground water levels, glacier advance or retreat, and sediment erosion or deposition, have long been known to modulate the rate of earthquake occurrence. Previous studies have documented this phenomenon at particular local- or regional-scale study areas. In Alaska, recent ice mass loss modulates seismicity at various

scales (*1–5*). Several studies have examined possible surface load triggering of earthquakes in Japan (*6–8*) and in California (*9, 10*). The occurrence of fewer earthquakes in the summer in Nepal compared to the winter has been attributed to surface mass loading (and unloading) in the Ganges and Northern India (*11–13*). Over longer timescales, tectonic stresses and stresses due to changes in glacier loading have been argued to explain earthquake activity in former glaciated shields of eastern Canada and Fennoscandia (*14*). Furthermore, episodic processes such as landslide erosion influences seismicity (*15*), a process that can be modeled as a transient normal stress change within a quasi-dynamic rate-and-state frictional sliding model (*16*). At the scale of individual faults, seismicity may additionally be associated with filling of surface reservoirs, although this phenomenon is complicated by pore pressure diffusion effects (*17*).

1 Global Datasets

In light of this literature relating surface loading to seismicity at the local- to regional-scale, we examine global datasets to quantify this relationship at a global scale. We examine mass concentration block (mascon) solutions from the Gravity Recovery and Climate Experiment (GRACE) and GRACE-Follow On (GRACE-FO) missions using the Jet Propulsion Laboratory GRCTellus product RL06M.MSCNv02 (*18–21*). These data have half-degree spatial sampling globally, although the underlying spatial resolution is 3 degrees. We examine GRACE and GRACE-FO data from April 2002 to January 2022. Each monthly mascon value represents the surface mass deviation for that month relative to Earth's static gravity field as inferred from a baseline average over the time period from January 2004 to December 2009.

We compare these surface loads to earthquake occurrence as quantified in the U.S. Geological Survey, Earthquake Hazards Program, Advanced National Seismic System (ANSS) Comprehensive Catalog of Earthquake Events (ComCat). We examine earthquakes in this catalog during the time period from April 2002 to January 2022 with magnitude greater than 5.4.

This magnitude threshold was chosen to reflect the approximate global magnitude of completeness (*22*). This subset of ComCat contains 12573 events.

Many earthquakes are clustered in the sense that they are triggered by previous earthquakes. Although these events could potentially bias our analysis, we find that the relationship between surface mass loading and earthquake occurrence is robust whether or not triggered events are included in the analysis. We decluster the USGS catalog using an Epidemic Type Aftershock (ETAS) model (*23*). The ETAS model results in an estimate of the probability that an earthquake is triggered by another earthquake. In our catalog, the mean and median probability of an event being triggered by another earthquake are 97.97% and 99.95%, respectively. In the rest of our analysis, we will focus on events that have less than 90% probability of being triggered. We will refer to the catalog of events that meet this requirement as the declustered catalog. Important to our purpose is that this ETAS model was shown by (*23*) to be more conservative in assigning triggering status compared to other, related methods. Application of the ETAS model with this probability cutoff resulted in a collection of 537 earthquakes that are not triggered (e.g., aftershocks).

2   Non-parametric Statistical Analysis and Results

We use non-parametric statistical tests to confirm the hypothesis that surface loads are significantly different during time periods with earthquakes as compared to arbitrary time periods. Non-parametric tests are useful because they make minimal assumptions about the underlying data distribution (*24*). The cumulative distribution and probability density plots relevant to our hypothesis are plotted in Figure 2a and b. Both the Kolmogorov-Smirnov (KS) test and the Cramer-von Mises (CvM) tests of distribution equality confirm the hypothesis (i.e., inequality of the distributions) with p-values of 6.21×10^{-37} and 3.14×10^{-3}, respectively, for the full catalog, and p-values of 1.08×10^{-3} and 3.17×10^{-9}, respectively, for the declustered cata-

log. We conclude that across different statistical tests (KS versus CvM) and catalog processing strategies (declustered versus full catalog), surface loads are systematically different during earthquake occurrence at no less than 99.6% confidence.

Next, we examine patterns in earthquake occurrence as a function of the amplitude of surface mass load. From the GRACE dataset, we directly calculate the probability of a given level of surface loading, P(surface load). Combined with the full earthquake catalog, we calculate the conditional probability of a given surface load during an earthquake occurrence, P(surface load | earthquake). With these two distributions in hand, we then use Bayes' theorem to calculate the conditional probability of an earthquake at a given surface load,

$$P(\text{earthquake} \mid \text{surface load}) = \frac{P(\text{surface load} \mid \text{earthquake}) \cdot P(\text{earthquake})}{P(\text{surface load})}. \tag{1}$$

In this analysis, we do not assume any form for the prior distribution $P(\text{earthquake})$. We therefore consider values of the conditional probability relative to the prior probability of an earthquake, i.e., the relative conditional probability $P(\text{earthquake} \mid \text{surface load})/P(\text{earthquake})$. When plotting the results of our Bayesian analysis, we use the Freedman-Diaconis Rule to calculate bin size (*25*), whereby the bin size is proportional to the interquartile range of the distribution.

We apply Bayes' theorem to both the full and declustered earthquake catalogs and plot the results in Figure 2c and f, respectively. The main result of our work, which is qualitatively true of both catalogs, is that the relative conditional probability of an earthquake is higher at large positive and negative surface mass loads. The symmetry of the resulting distribution, i.e., that the probability of an earthquake is elevated at both large negative and positive mass loads, is an important feature of our results that we discuss later.

Earthquakes are more than twice as likely at extreme values of surface loading (±15 cm-we; Figure 2f) in the declustered catalog. We use this result to form a criterion for an earthquake to

be categorized as a surface load induced earthquake (SLIQ). Most earthquakes have a relative conditional probability near unity (median: 1.06 cm-we, interquartile range: 0.68 cm-we), as expected if most earthquakes are not induced by surface loads. We therefore set a relative conditional probability of 1.74 to be our threshold for the definition of a SLIQ to examine events in the upper quartile of relative conditional probability. From our declustered catalog of 537 earthquakes, 49 have relative conditional probabilities greater than 1.74 and 27 have a relative conditional probabilities greater than 2.0.

The spatial pattern of the SLIQs is plotted in Figure 1. The map shows most SLIQs occurring along the collision zones of the southern margin of the Eurasian plate. Additional SLIQ activity is seen in North America, sub-Saharan Africa, and East Asia. Most identified SLIQs are on land but a few are oceanic. We consider the prevalence of SLIQs in the broader India-Eurasian and Alaskan plate boundaries to represent a generalization of previous studies of seasonal seismicity in these regions (*1, 2, 11–13*). We find that most of the SLIQs occur at mid latitude, around continental collision zones. This suggests that the SLIQs are occurring at regions which experience a relatively large climatic induced surface load at tectonically active regions. In contrast, few SLIQs occur in subduction zones or along mid ocean ridges.

We find the largest magnitude SLIQ to be the 2015 Gorkha Earthquake (*26, 27*) and the 2011 Sikkim Earthquake (*28*). These SLIQs occurred during surface loads of 15.51 cm-we and 11.20 cm-we, respectively. The SLIQs that had the highest relative conditional probability, given the surface loading, occurred in India in 2005 (M 5.8), the India-Bangladesh border in 2003 (M 5.7), and eastern Xizang along the India-China border (M 5.5). These events all have a relative conditional probability of 11.91. Other notable events in our SLIQ catalog include the 2017 Montana earthquake (*29*), which has a relative conditional probability of 2.35 given that it occurred at a surface load of -10.38 cm-we.

3 Discussion

SLIQs occur with both negative and positive extreme loading (Figure 2c and f). This symmetry could plausibly be explained by faulting style if positive and negative surface loads are correlated with normal and thrust fault motion, respectively. In order to test this hypothesis and to better understand this symmetry, we therefore analyze the focal mechanisms of the 49 SLIQs from the declustered catalog. Out of these 49 events only 25 had catalogued focal mechanisms. For each of these 25 SLIQs, we examine the vertical component of the slip direction vector,

$$U_{\text{vertical}} = \sin(\delta)\sin(\lambda), \tag{2}$$

with fault dip δ and fault rake λ. We find that 11 out of 13 thrust fault SLIQs ($U_{\text{vertical}} > 0$) occurred during a time with a negative surface mass load. In contrast, 6 normal fault SLIQs ($U_{\text{vertical}} < 0$) occurred with positive load and 6 occurred with negative load. From this analysis, we conclude that there is moderately strong evidence that the symmetry of the SLIQ surface load response is correlated with faulting style.

The existence of SLIQs suggests novel interactions between cascading hazards. The 2015 Gorkha earthquake, for example, triggered more than 20,000 landslides across 14 districts of Central and Western Nepal (*30*). At the same time, our analysis here as well as previous modeling studies provide evidence for the hypothesis that such landsliding activity may in turn modify earthquake nucleation (*16*), suggesting that cascading solid Earth and Earth-surficial hazards exhibit two-way coupling.

The existence of SLIQs fills in a temporal- and spatial-gap in the spectrum of solid Earth–fluid Earth interaction. Analogous studies have shown, for example, that global volcanism is modulated by surface loads at time scales ranging from hours to hundreds of thousands of years (*31*). For earthquakes, there is evidence to suggest that glacial-interglacial fluctuations in lithospheric rebound can modify normal fault slip rate (*32*). We have demonstrated that surface

6

loading triggering of earthquakes is a global-scale phenomenon at the monthly timescale.

References

1. J. Sauber, G. Plafker, B. F. Molnia, M. A. Bryant, *Journal of Geophysical Research: Solid Earth* **105**, 8055 (2000).

2. J. M. Sauber, B. F. Molnia, *Global and Planetary Change* **42**, 279 (2004).

3. D. I. Doser, K. R. Wiest, J. Sauber, *Tectonophysics* **439**, 119 (2007).

4. C. W. Johnson, Y. Fu, R. Bürgmann, *Earth and Planetary Science Letters* **530**, 115904 (2020).

5. C. Rollins, J. T. Freymueller, J. M. Sauber, *Journal of Geophysical Research: Solid Earth* **126**, e2020JB020411 (2021).

6. K. Heki, *Earth and Planetary Science Letters* **207**, 159 (2003).

7. Y. Mitsui, K. Yamada, *Earth, Planets and Space* **69**, 1 (2017).

8. L. Xue, *et al.*, *Journal of Geophysical Research: Solid Earth* p. e2021JB023301 (2021).

9. S. S. Gao, P. G. Silver, A. T. Linde, I. S. Sacks, *Nature* **406**, 500 (2000).

10. L. B. Christiansen, S. Hurwitz, S. E. Ingebritsen, *Geophysical Research Letters* **34** (2007).

11. L. Bollinger, *et al.*, *Geophysical Research Letters* **34** (2007).

12. P. Bettinelli, *et al.*, *Earth and Planetary Science Letters* **266**, 332 (2008).

13. S. Kannaujiya, *et al.*, *Quaternary International* **575**, 62 (2021).

14. I. S. Stewart, J. Sauber, J. Rose, *Quaternary Science Reviews* **19**, 1367 (2000).

15. P. Steer, *et al.*, *Scientific reports* **10**, 1 (2020).

16. L. Jeandet Ribes, N. Cubas, H. S. Bhat, P. Steer, *Geophysical Research Letters* **47**, e2020GL087631 (2020).

17. E. A. Roeloffs, *Journal of Geophysical Research: Solid Earth* **93**, 2107 (1988).

18. M. M. Watkins, D. N. Wiese, D.-N. Yuan, C. Boening, F. W. Landerer, *Journal of Geophysical Research: Solid Earth* **120**, 2648 (2015).

19. D. N. Wiese, F. W. Landerer, M. M. Watkins, *Water Resources Research* **52**, 7490 (2016).

20. D. Wiese, D. Yuan, C. Boening, F. Landerer, M. Watkins, *DAAC: Pasadena, CA, USA* (2018). Dataset accessed 2021-05-01 at http://dx.doi.org/10.5067/TEMSC-3MJC6.

21. F. W. Landerer, *et al.*, *Geophysical Research Letters* **47**, e2020GL088306 (2020).

22. J. Woessner, S. Wiemer, *Bulletin of the Seismological Society of America* **95**, 684 (2005).

23. L. Mizrahi, S. Nandan, S. Wiemer, *Seismological Society of America* **92**, 2333 (2021).

24. G. W. Corder, D. I. Foreman, *Nonparametric statistics: A step-by-step approach* (John Wiley & Sons, 2014).

25. D. Freedman, P. Diaconis, *Zeitschrift für Wahrscheinlichkeitstheorie und verwandte Gebiete* **57**, 453 (1981).

26. J.-P. Avouac, L. Meng, S. Wei, T. Wang, J.-P. Ampuero, *Nature Geoscience* **8**, 708 (2015).

27. M. A. Denolle, W. Fan, P. M. Shearer, *Geophysical Research Letters* **42**, 7467 (2015).

28. S. Baruah, A. Bramha, S. Sharma, S. Baruah, *Natural Hazards* **97**, 1001 (2019).

29. N. D. McMahon, *et al.*, *Seismological Research Letters* **90**, 131 (2019).

30. N. Rosser, *et al.*, *Progress in Disaster Science* **10**, 100159 (2021).

31. P. Huybers, C. Langmuir, *Earth and Planetary Science Letters* **286**, 479 (2009).

32. R. Hetzel, A. Hampel, *Nature* **435**, 81 (2005).
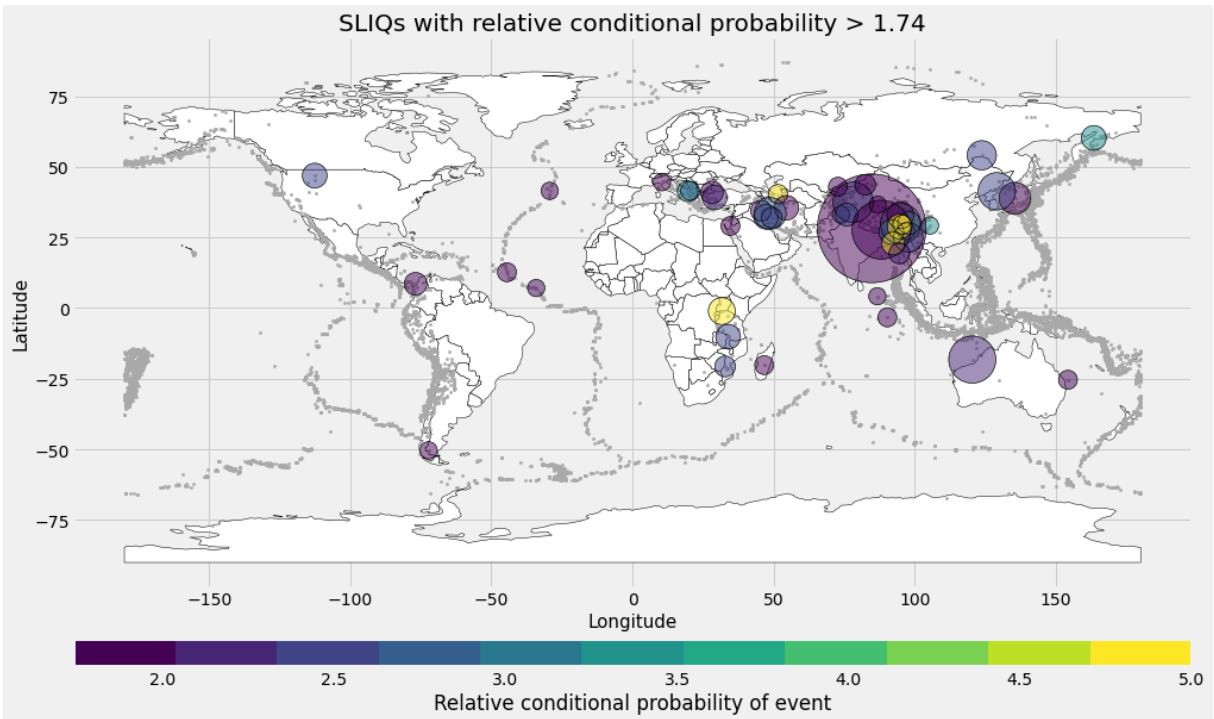
Acknowledgments

Figure 1: Earthquakes (magnitude > 5.4) with a relative conditional probability > 1.74. The events were recorded by the USGS ANSS ComCat earthquake catalog from April 2002 to January 2022. The earthquake magnitude is denoted by circle size and relative conditional probability by color. The small gray dots represent all the earthquakes in our initial catalog which is a subset of ComCat containing 12573 events.
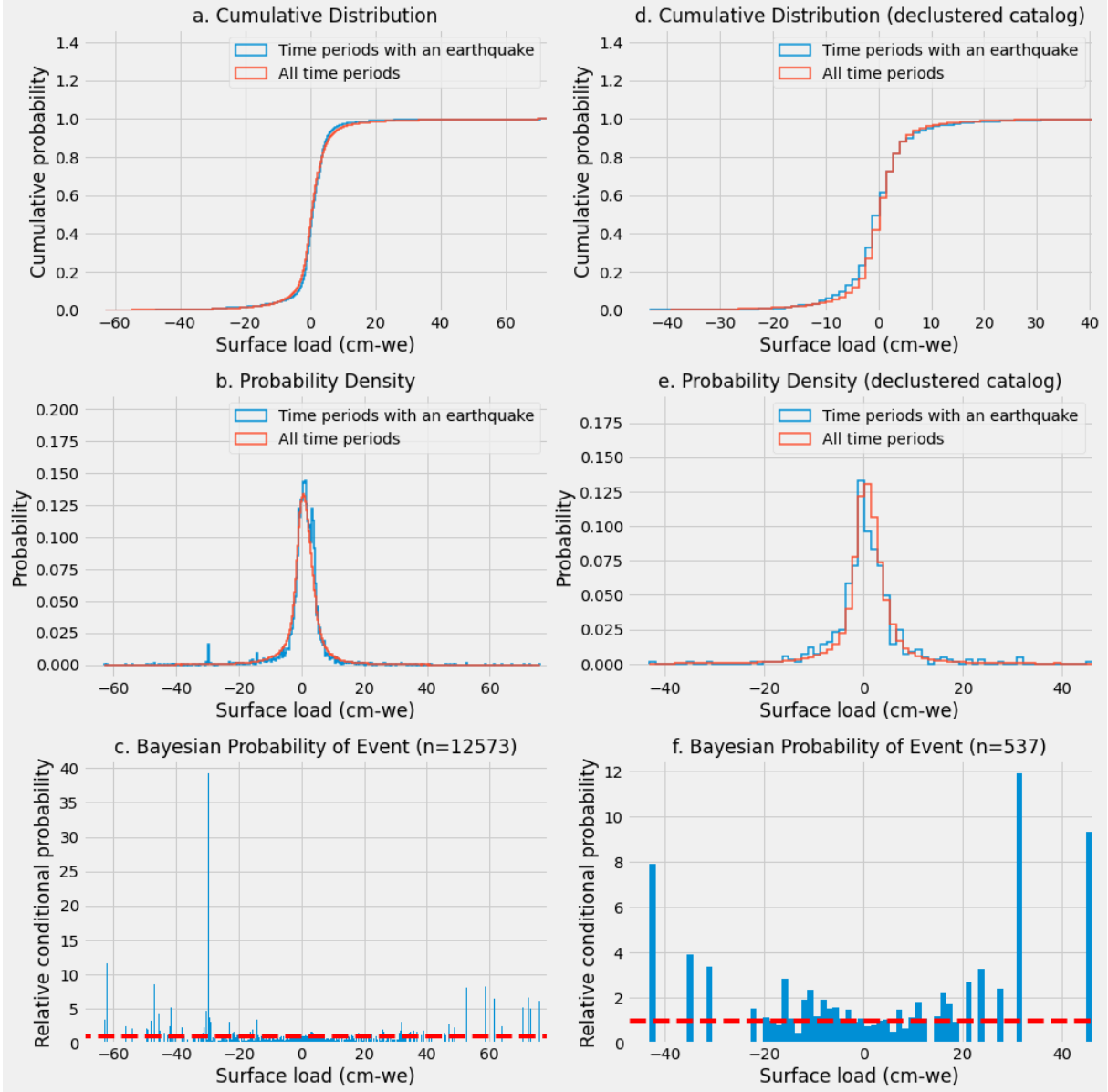
Figure 2: (a) The cumulative distribution of global surface mass loading during all time periods (red) and during time periods with an earthquake occurrence (blue) (b) The probability density of global surface mass loading during all time periods (red) and during time periods with a earthquake occurrence (blue) (c) The relative conditional probability of a earthquake occurrence given a value of surface mass load. The histogram represents the relative conditional probabilities for 12573 events. The red line represents where the probability of an earthquake given a value of surface loading (P(earthquake|surface load)) is equal to the probability of an earthquake (P(earthquake)) (d,e,f) These figures represent the same relationships as (a),(b), and (c) for the declustered catalog with 537 events

11